Geophysical Research Letters

RESEARCH LETTER
10.1029/2023GL104431

Observation of Non-Resonance Interactions Between Cold Protons and EMIC Waves of Different Polarizations in the Inner Magnetosphere

Xinmin Li[1,2,3], Rongsheng Wang[1,2,3], Xinliang Gao[1,2,3], Quanming Lu[1,2,3], Huayue Chen[4], and Jiuqi Ma[1,2,3]

[1]Deep Space Exploration Laboratory/School of Earth and Space Sciences, University of Science and Technology of China, Hefei, China, [2]CAS Center for Excellence in Comparative Planetology/CAS Key Laboratory of Geospace Environment/Anhui Mengcheng National Geophysical Observatory, University of Science and Technology of China, Hefei, China, [3]Collaborative Innovation Center of Astronautical Science and Technology, Harbin, China, [4]Department of Physics, Auburn University, Auburn, AL, USA

Key Points:

- Both the left-hand and right-hand polarized electromagnetic ion cyclotron (EMIC) waves can interact with cold protons via non-resonance interaction
- The cold protons experience different types of phase bunching with different polarizations of EMIC waves
- The energy transfer process is not affected by the polarization of EMIC waves

Supporting Information:

Supporting Information may be found in the online version of this article.

Correspondence to:

R. Wang,
rswan@ustc.edu.cn

Citation:

Li, X., Wang, R., Gao, X., Lu, Q., Chen, H., & Ma, J. (2023). Observation of non-resonance interactions between cold protons and EMIC waves of different polarizations in the inner magnetosphere. *Geophysical Research Letters*, *50*, e2023GL104431. https://doi.org/10.1029/2023GL104431

Received 4 MAY 2023
Accepted 25 OCT 2023

Abstract Using the high-quality measurements of plasma by the Magnetospheric Multiscale (MMS) spacecraft, we investigate the wave-particle interaction between cold protons and Electromagnetic ion cyclotron (EMIC) waves of different polarizations in the inner magnetosphere. Both the left-hand and right-hand polarized EMIC waves can interact with cold protons via non-resonance interaction, and energize the cold protons (~eV) up to suprathermal energies (~tens of eV), resulting in a series of bridge-like arcs in the ion energy spectrogram. Cold protons experience different types of phase bunching in left-hand and right-hand polarized EMIC waves. However, the relative angles between the velocities of bunched protons and wave magnetic or electric fields are independent of the polarizations of EMIC waves. Thus, the energy transfer process is not affected by the polarization of EMIC waves. The observations indicate that EMIC waves can affect the magnetospheric particle dynamics by energizing the cold protons.

Plain Language Summary Electromagnetic ion cyclotron (EMIC) waves play an important role in the magnetospheric particle dynamics via wave-particle interactions. Previous studies mainly focus on the resonance interaction between particles and EMIC waves. The resonance interaction is effective but it needs the energy of particles to be above the minimum resonant energy. In our observation, we find that the cold protons (~eV) are energized up to suprathermal energies (~tens of eV) by the EMIC waves, resulting in a series of bridge-like arcs in the ion energy spectrogram. The energy of cold protons is much less than the minimum resonant energy, suggesting that the cold protons should be energized by the non-resonance interaction. The polarization of EMIC waves could change the gyrophase distribution of bunched cold protons, but the energy transfer process is not affected by the polarization of EMIC waves. The observations suggest EMIC waves can affect the magnetospheric particle dynamics by energizing the cold protons.

1. Introduction

Electromagnetic ion cyclotron (EMIC) waves are electromagnetic emissions with frequencies belonging to Pc1-Pc2 geomagnetic pulsations (0.1–5 Hz) (Anderson et al., 1992; Cornwall, 1965; D. Young et al., 1981). They are frequently observed in the terrestrial magnetosphere, and are predominantly excited by cyclotron instability of energetic protons (~10–100 keV) with anisotropic temperature distributions ($T_{i,\perp} > T_{i,\parallel}$) in the vicinity of the geomagnetic equator (L. Chen et al., 2011; Cornwall, 1965; Gary et al., 2012; Kennel & Petschek, 1966; Q. Lu et al., 2006; Teng et al., 2019; Xiao et al., 2007; Yue et al., 2019). The newly generated EMIC waves are predominantly left-hand polarization and propagate along the background magnetic field. As they propagate away from the source region, their wave normal angles become oblique and the polarization could deviate from left-hand polarization (Allen et al., 2015; H. Chen et al., 2019; Hu et al., 2010; Kang et al., 2021; E. H. Kim & Johnson, 2016). Moreover, it has been suggested that the generation and propagation of EMIC waves in the terrestrial magnetosphere could be affected by the solar wind pressure and substorm injection (H. Chen et al., 2020; L. Chen et al., 2014; Jordanova et al., 2001; McCollough et al., 2012; Meredith et al., 2014; Usanova et al., 2012).

The EMIC waves are supposed to play an important role in the magnetospheric particle dynamics via wave-particle interactions. For example, EMIC waves can interact with energetic (~keV) ions and relativistic (~MeV) electrons

through resonant wave-particle interactions, by which particles can precipitate into the atmosphere, leading to the formation of auroras (Carson et al., 2013; Gao et al., 2015; N. Kitamura et al., 2021; W. Li et al., 2007; Ni et al., 2015; Thorne & Kennel, 1971; Xiao et al., 2011; Yuan et al., 2012; X. J. Zhang et al., 2016). The EMIC wave can also produce significant pitch angle scattering of hundred-keV electrons by the non-resonant interaction, when the wave packets are short (An et al., 2022; L. J. Chen et al., 2016).

In addition, a close correlation between the occurrence of EMIC waves and cold He^+ ions heating was found in previous observations (K H Kim et al., 2021; Lee et al., 2021; D Young et al., 1981; J. C. Zhang et al., 2011). The cold He^+ ions can be energized by EMIC waves up to suprathermal energies (tens of eV to a few hundred eV) in the perpendicular direction to the background magnetic field (K. H. Kim et al., 2022; Omidi et al., 2010; Shi et al., 2020; Yuan et al., 2016). The energy of the cold He^+ ions is much lower than the typical minimum resonant energy of EMIC waves, thus, the energy transfer between cold He^+ ions and EMIC waves should also be a non-resonant interaction mechanism, which has been explored in theory and numerical simulation (Berchem & Gendrin, 1985; Bortnik et al., 2010; Mauk, 1982; Omura et al., 1985). Limited by the resolution of particle measurement, the observational evidence of non-resonant interaction is lacking before the launch of Magnetospheric Multiscale mission (MMS) (Burch et al., 2016). Based on the extremely high time resolution measurement by MMS, a few observations have shown that the cold ions could experience phase bunching with the EMIC waves, and leading to the energy exchange between them (N. Kitamura et al., 2018; J.-H. Li et al., 2022; Z.-Y. Liu et al., 2022), which was consistent with the previous predictions of the non-resonant interaction (Bortnik et al., 2010). However, previous studies just forced on the non-resonant interaction between left-hand polarized EMIC and cold ions. The effect of wave polarization needs to be taken into account to fully understand the non-resonant interaction between cold ions and EMIC waves.

In this paper, we investigated a train of EMIC waves in the inner magnetosphere. The polarizations of EMIC waves reversed three times within about 24 periods of waves, thus, the interactions between cold ions and EMIC waves of different polarizations can be examined simultaneously.

2. Instrumentations

The data used in this paper was measured by Magnetospheric Multiscale mission (MMS). The magnetic fields and electric fields used in this paper were measured by Flux Gate Magnetometer (FGM) (Russell et al., 2016)with a time resolution of 16 Hz (survey mode) and electric field double probe (EDP) (Ergun et al., 2016; Lindqvist et al., 2016) with a time resolution of 128 Hz (fast survey mode), respectively. The 3-D ions distribution functions and ions moments data were taken from Fast Plasma Investigation (FPI) (Pollock et al., 2016) with the time resolution of 150 ms. The Hot Plasma Composition Analyzer (HPCA) (D T Young et al., 2016) provided the information of ions composition. During this event, the measurements of the four spacecraft were almost the same. Thus, the data from MMS1 were only used in this paper.

3. Observation and Analysis

3.1. Overview of EMIC Waves and Cold Protons Energization

Figure 1 presents an overview of EMIC waves on 05 January 2019, when MMS spacecraft was located at the inner magnetosphere (L-shell = 9.0) and close to the noonside geomagnetic equator (magnetic local time = 11.3 and magnetic latitude = −1.6, shown at the bottom of Figure 1). Figure 1a shows the wave magnetic spectrogram in the frequency range of 0.1–10 Hz, with the solid black traces representing the local H^+ (f_{H^+}) and He^+ (f_{He^+}) gyrofrequencies. Between f_{He^+} and f_{H^+}, the waves with the peak frequency at around 0.37 Hz ($0.33 f_{H^+}$) were identified. With the three components of magnetic field measurement, the wave power of left-hand (P_L) and right-hand (P_R) modes can be separated (E. H. Kim & Johnson, 2016; J. C. Zhang et al., 2011). The wave powers of left-hand and right-hand mode waves, and their comparison at the wave peak frequency (~0.37 Hz) were shown in Figures 1b–1d. From 09:24:40.0 to 09:24:50.0 UT, and from 09:24:58.8 to 09:25:10.0 UT, the wave power of right-hand mode (P_R, red traces in Figure 1d) was dominant over the left-hand mode (P_L, blue traces in Figure 1d), suggesting that the waves were right-hand polarized in these periods. But for the remainder, the waves were left-hand polarization, because of $P_L > P_R$. The wave normal angles (WNAs, shown in Figure 1e) were predominantly small (<30°), indicating that the waves propagated primarily along the magnetic field lines. However, at around 09:24:50.0 UT, 09:24:58.8 UT, and 09:25:10.0 UT, when the polarization reversals occurred,

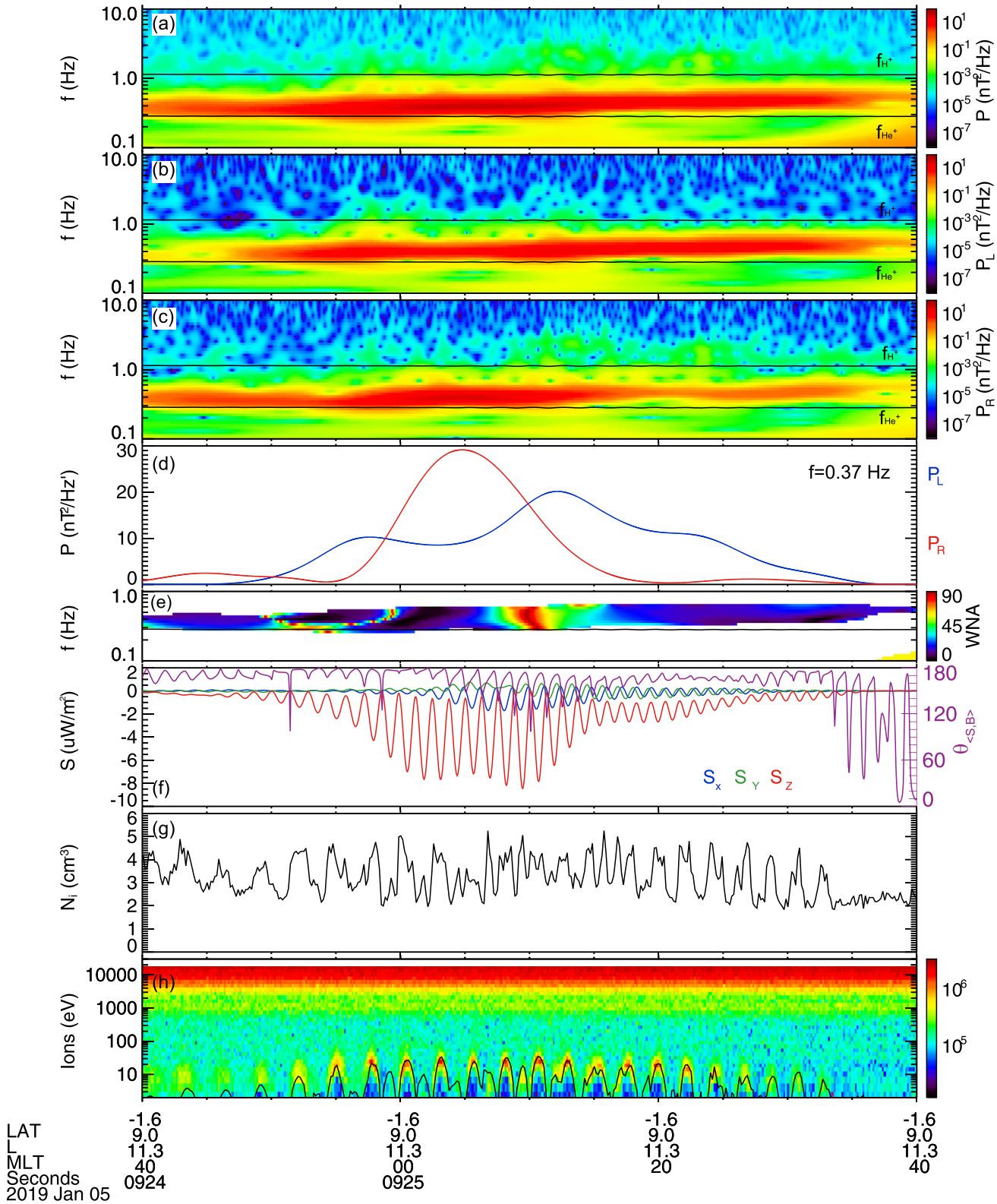

Figure 1. Overview of the EMIC waves. (a)–(c) wave magnetic power spectrograms of total, left-hand polarized and right-hand polarized mode according to wavelet technique. (d) Comparison of the left-hand (blue trace) and right-hand polarized wave power at frequency of 0.37 Hz. (e) Wave normal angle within frequency range of 0.1–1 Hz. (f) The Poynting fluxes FAC coordinates, and the magenta traces show the angle between Poynting fluxes direction and background magnetic fields. (g) Ion number density from dis-partmoms data including ions from all energy channels. (h) Ion energy spectrogram with the energy of $\mathbf{E} \times \mathbf{B}$ drift. The black transverse traces superposed on (a)–(c) represent local He+ ($f_{He^+} \sim 0.28$ Hz) and H+ ($f_{H^+} \sim 1.13$ Hz) gyrofrequencies.

WNAs became large and even reached 90°, indicating that the propagation of waves was oblique and even perpendicular to the background magnetic field, which was supported by the Poynting fluxes in Figure 1f. In addition to the polarization reversal points, the direction of the Poynting fluxes were almost anti-parallel to the background magnetic field (Z-FAC), indicating that both the left-hand and right-hand waves were mainly propagating in the anti-parallel direction, that is, propagating to higher latitudes. Based on the above observations, these waves were identified as Hydrogen band EMIC waves, and the polarization reversal of these waves occurred three times within one minute (about 24 periods of waves).

Meanwhile, the differential energy flux of cold ions with energy less than 40 eV increased periodically at the same frequency of the waves. Thus, a series of bridge-like arcs were observed in the ion energy spectrogram (Figure 1h). The periodic enhancements of cold ions flux resulted in the ions number density measured by FPI periodically increasing from ~2 cm^{-3} up to 4–5 cm^{-3} (Figure 1g). Moreover, the HPCA data provided the information of ions composition, which suggests that the total number density of heavy ions (n_{He+} = 0.0002 cm^{-3}; n_{O+} = 0.013 cm^{-3}) was only 1% of that of protons. Thus, the ions behaviors detected by FPI were dominant by protons. The coincident frequency between waves and the enhancements of cold proton number density suggests that the cold protons should be modulated by the EMIC waves. The energies of the cold protons were close to the energy of $\mathbf{E} \times \mathbf{B}$ drift (less than 40 eV, the black traces in Figure 1h or 2a), which is similar to the previous observations of ULF waves (Z. Y. Liu et al., 2019). In the following section, the wave-particle interactions between EMIC waves and cold protons at energies less than 40 eV will be studied.

3.2. Wave-Protons Interactions

To further investigate the waves, the magnetic and electric fields of EMIC waves in the field-aligned coordinate (FAC) system were shown in Figures 2b and 2c, respectively. The wave magnetic ($\mathbf{B}_{wave}$) and electric ($\mathbf{E}_{wave}$) fields were produced from fast survey mode FGM (magnetic field) data and EDP (electric field) data, by a band-pass filter with a frequency range of 0.3–0.5 Hz. The FAC system was determined based on the sunward direction ($\mathbf{X}_{gse}$ direction in the Geocentric Solar Ecliptic (GSE) coordinates system) and background magnetic field, which was obtained from FGM data by a low-pass filter at the frequency below 0.1 Hz. $\mathbf{Z}$ was along the direction of the background magnetic field. $\mathbf{Y}$ was calculated by the cross product of $\mathbf{Z}$ and $\mathbf{X}_{gse}$, and $\mathbf{X}$ completed the right-hand system. The change of phase difference between B_x and B_y in the FAC system also suggested that the polarization reversals occurred at around 09:24:50.0 UT, 09:24:58.8 UT, and 09:25:10.0 UT, consistent with the preceded analysis of relative power of left-hand and right-hand mode waves (Figure 1d).

There was a background electric field in this event, which caused the plasma to have a background drift velocity. To remove the influence from the background electric field drift, the following analyses were carried out in the plasma rest frame (the details of the frame transformation process can be found in Supporting Information S1).

Figure 2e shows the pitch angle distributions of cold protons (0–40 eV) in the rest frame of the plasma. When the EMIC waves were weak (09:24:40.0–09:24:50 UT, and 09:25:35.0–09:25:40 UT), the cold protons were mainly observed in the direction parallel or antiparallel to the background magnetic fields, indicating that the cold protons came from the ionosphere outflow (Z Y Liu et al., 2019). When the EMIC waves became intense, and the bridge-like arcs were clearly observed in the ion energy spectrogram (Figure 2a), the flux enhancements were observed around 90° in the pitch angle distribution, suggesting that the cold protons were accelerated in the direction perpendicular to the background magnetic field, consistent with the previous observations (K H Kim et al., 2021; Yuan et al., 2016). Figure 2f shows the gyrophase distributions of the cold protons with energies 0–40 eV and with the pitch angles of 60°–120°. The gyrophase distribution was based on the FAC coordinate system, and the gyrophase angles equal to 0° represented the X-FAC direction in the XY-FAC plane. Two types of gyrophase distributions were observed, and they were related to the polarization of the EMIC waves. When the waves were right-hand polarized (09:24:40.0–09:24:50.0 UT, and 09:24:58.8–09:25:10.0 UT), the gyrophase of periodic cold protons was mostly stable at about 220°, with a small percentage around 50°. While, when the waves were left-hand polarized (09:24:50.0–09:24:58.8 UT, and 09:25:10.0–09:25:40.0 UT), the gyrophase of periodic cold protons was rotating from 360° to 0°. The observations suggest that the cold protons were phase bunched, and the types of phase bunching were affected by the polarizations of EMIC waves. Moreover, the bunched cold protons exhibited agyrotropic gyrophase distributions, indicating that the energy conversion was ongoing between cold protons and EMIC waves.

To reveal the interaction between the cold protons and EMIC waves, wave-particle interaction analysis (WPIA) (Fukuhara et al., 2009) was applied to investigate the energy transfer rate between cold protons and EMIC waves.

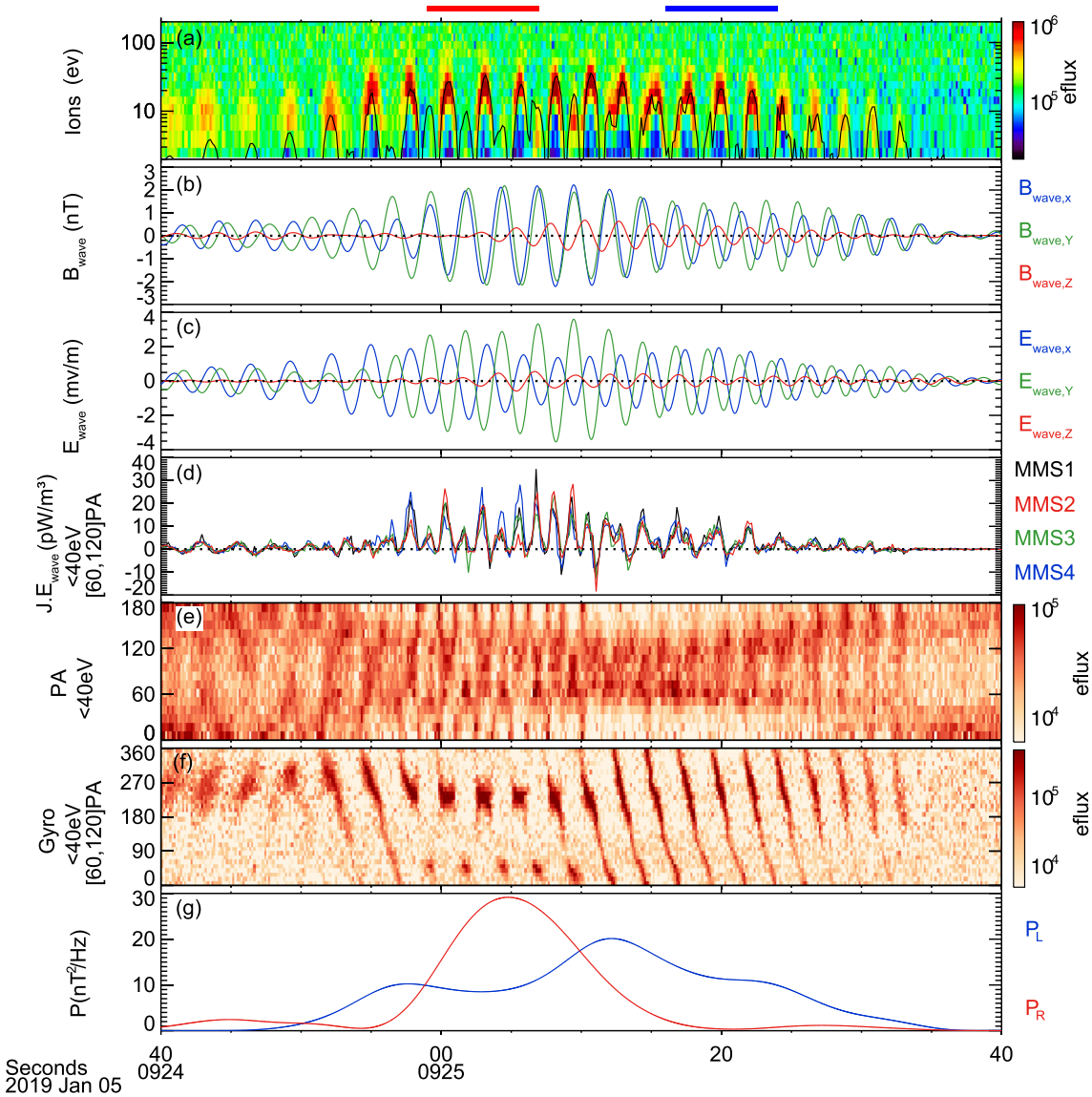

Figure 2. Energy Transference from EMIC waves to cold Protons. (a) Ion energy spectrogram. (b) Wave magnetic field in the field-aligned coordinates. (c) Wave electric field in the field-aligned coordinates. (d) Energy conversion rate between EMIC wave and ions, $J_i \cdot E_{wave}$ from four MMS spacecraft, where J_i is the current supported by ions with energy range of 0–40 eV and pitch angle of 60–120°, and E_{wave} is wave electric field. (e) Pitch angle distribution for ions with energy range of 0–40 eV. (f) Gyro-phase spectrogram for ions with energy range of 0–40 eV and pitch angle of 60–120°. (g) Comparison of the left-hand (blue trace) and right-hand polarized wave power at frequency of 0.37 Hz. Both the energy conversion rate, pitch angle distribution, and gyro-phase distribution were calculated in the plasma rest frame.

The energy transfer rate was calculated by the dot product of the electric field of EMIC waves ($\mathbf{E}_{wave}$) and ion current ($\mathbf{J}_i$). The ion current was supported by the cold protons with energies less than 40 eV and pitch angles 60°–120°, and calculated as $\mathbf{J}_i = q_i \cdot N_i \cdot \mathbf{V}_i$ (q_i is the proton's charge, N_i and $\mathbf{V}_i$ are number density and velocity of cold protons with energies 0–40 eV and pitch angles 60°–120° in the rest frame of the plasma). As shown in Figure 2d, the energy transfer rate, $\mathbf{J_i} \cdot \mathbf{E}_{wave}$, exhibited quasiperiodic oscillations, and they were nearly consistent for all four MMS spacecraft. $\mathbf{J_i} \cdot \mathbf{E}_{wave}$ was always positive when the cold protons flux enhancements occurred, indicating that the energy transferred from EMIC waves to cold protons, that is, the cold protons were energized by the EMIC waves. It was surprising that the cold protons could be energized by EMIC waves regardless of the wave polarization, although the gyrophase distributions of bunched cold protons were different with different polarizations of EMIC waves (Figure 2f).

To investigate the effect of the wave polarization variation on the cold proton energization, Figure 3 shows the comparison of the cold proton behavior with the left-hand (left column, blue shadow region in Figure 2) and

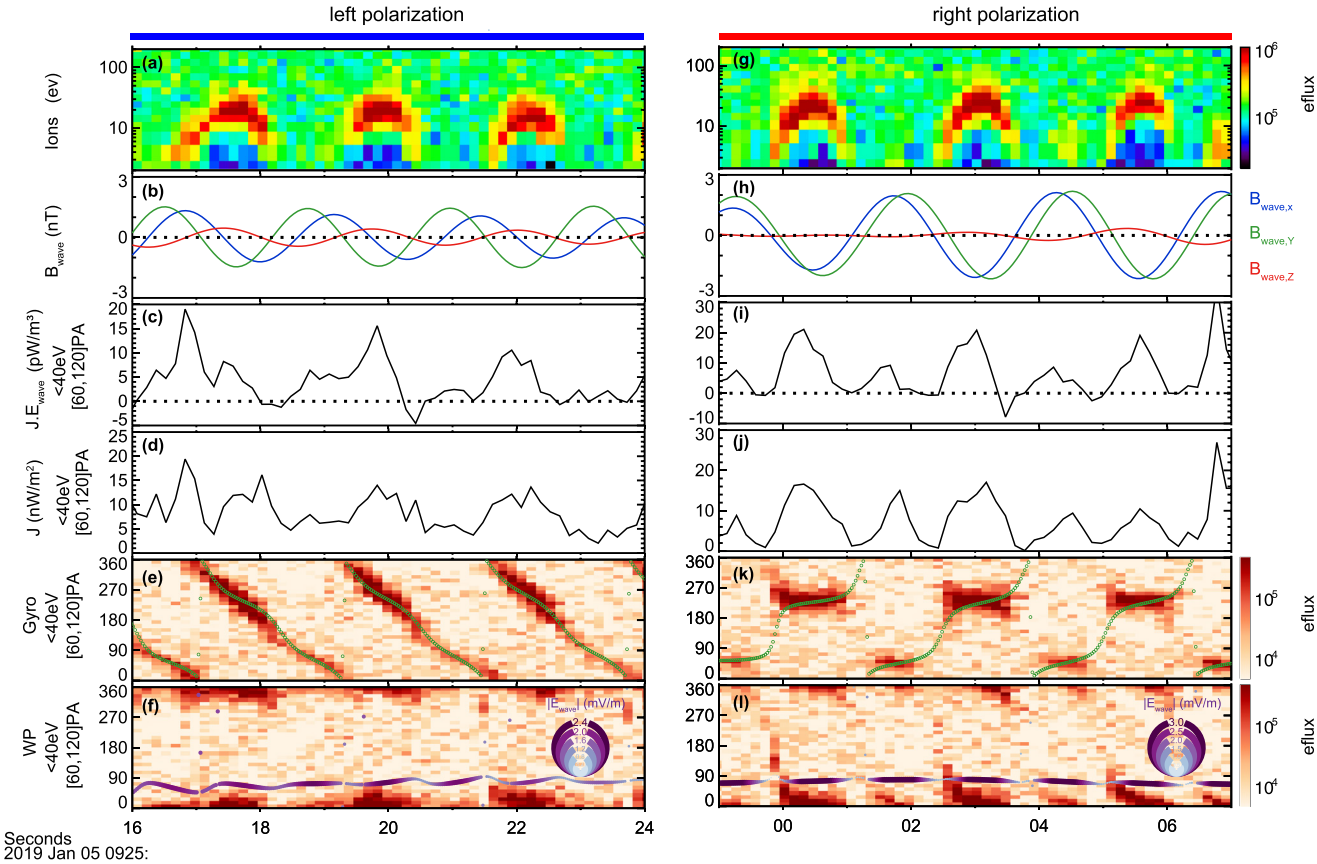

Figure 3. Comparison of the cold protons behaves in the left-hand and right-hand polarized wave. The left and right columns correspond to left-hand and right-hand polarized wave, respectively. (a) Ion energy spectrogram. (b) Wave magnetic field in the field-aligned coordinates. (c) Energy conversion rate between EMIC wave and ions, (d) current density, supported by ions with energy range of 0–40 eV and pitch angle of 60–120°, (e) Gyro-phase spectrogram for ions with energy range of 0–40 eV and pitch angle of 60–120°. Green circles represent the direction of B_{wave}. (f) Relative phase spectrogram for ions with energy range of 0–40 eV and pitch angle of 60–120°. Purple circles represent the direction of E_{wave}, and the intensity and radius of the circles depends on the magnitude of E_{wave}. (g–l) The data in the same format of (a)–(f).

right-hand (right column, red shadow region in Figure 2) polarized EMIC waves. The gyrophase distributions of cold protons were shown in Figures 3e and 3k, with the green circles representing the directions of wave magnetic fields in the XY (FAC coordinates system) plane. For the left-hand polarized EMIC waves, the wave magnetic field rotated from 360° to 0° (left-hand rotation). The bunched cold protons followed the rotation of wave magnetic fields. But, as shown in wave-phase angle distributions (Figure 3f), there was a phase difference between $\mathbf{B}_{wave}$ and the bunched cold protons (Figure 3f). The wave-phase angle was defined as the relative phase angle between the velocities of cold protons and $\mathbf{B}_{wave}$ in the rest frame of the plasma. The wave-phase angles of the bunched cold protons were around 0° (or 360°), with a tendency toward 90°. Namely, the highest concentration of bunched cold protons was observed at the wave-phase angle between 0° and 90° (~20°). Meanwhile, the wave electric fields were superposed in Figure 3f by the purple cycles, and the color depth and radius of the circles were proportional to the magnitude of $\mathbf{E}_{wave}$. The relative phase angles between $\mathbf{E}_{wave}$ and $\mathbf{B}_{wave}$ nearly remained at around 90°. Thus, the relative angles between $\mathbf{E}_{wave}$ and the velocities of the most bunched cold protons were less than 90°, leading to the energy transfer from EMIC waves to cold protons ($\mathbf{J}_i \cdot \mathbf{E}_{wave} = qn_i \mathbf{V}_i \cdot \mathbf{E}_{wave} > 0$, as shown in Figure 3c). Moreover, the flux of cold protons just increased when the wave electric field was strong (Figure 3f), indicating that the cold ions should be modulated by the wave electric field.

For the right-hand polarized waves, the wave magnetic field rotated from 0° to 360° (right-hand rotation), and the gyrophase of bunched cold protons was mostly stable at about 220°, with a small percentage around 50° (shown in Figure 3k). The relative phase angles between $\mathbf{B}_{wave}$ and bunched cold protons were similar to those in the left-hand polarized waves, and the most bunched cold protons were observed at the wave-phase angle between 0° and 90° (Figure 3l). With $\mathbf{E}_{wave}$ remaining at around 90°, the bunched cold protons were also energized by the

right-hand polarized EMIC waves. Although the behaviors of bunched cold protons were different for different polarized EMIC waves, the angles between $\mathbf{E}_{\text{wave}}$ and the velocities of most bunched cold protons were always less than 90°, leading to the energy transfer from waves to cold protons ($\mathbf{J_i}\cdot\mathbf{E}_{\text{wave}} = qn_i\mathbf{V_i}\cdot\mathbf{E}_{\text{wave}} > 0$). Moreover, the energy transfer process was modulated by the wave electric field, and it became evident only when the wave electric field was intense. In summary, the cold protons could be energized by the EMIC waves, regardless of the polarizations of EMIC waves, and the wave electric field played a key role in the energization process.

4. Discussion and Conclusions

In this paper, we investigated a train of EMIC waves in the inner magnetosphere at $L = 9.0$ and their interaction with the cold protons at energies less than 40 eV, based on the MMS measurements. The behaviors of cold protons within one EMIC wave period are revealed clearly. Moreover, the polarization of the EMIC waves reversed three times within one minute, ∼24 periods of the EMIC waves. Thus, the interaction between cold ions and EMIC waves of different polarizations were investigated simultaneously.

It is well known that the EMIC waves were predominantly left-hand polarized with small wave normal angles when they were generated at around the geomagnetic equator. As they propagated along the background magnetic field to higher magnetic latitudes, they could undergo polarization reversal where the local crossover frequency equaled to the wave frequency (Allen et al., 2015; Hu et al., 2010). In our event, however, the EMIC waves underwent polarization reversal three times within a short period (about 24 EMIC wave periods), just at around the geomagnetic equator (MLAT = −1.6). Furthermore, the extremely low densities of heavy ions caused the crossover frequency ($f_{co} \sim 0.28$ Hz $\sim 0.25 f_{H^+}$) to be very low, almost equal to the He^+ gyrofrequency, which was much smaller than the peak frequency of EMIC waves ($f_{peak} = 0.37$ Hz). Thus, the reason for the polarization reversals may be different from the mode conversion at the cross-over frequency. It is worth noting that each reversal was accompanied by the oblique wave normal angles, with some even reaching 90°, indicating that the occurrence of polarization reversal at around the geomagnetic equator may be associated with the oblique propagation (Horne & Thorne, 1997; Hu & Denton, 2009; Rauch & Roux, 1982). Moreover, it has been found that the low abundance ratio of He+ ions (Denton et al., 1992; Hu & Denton, 2009) can excite the right-hand polarization EMIC waves in the source region. In our event, the abundance ration of He+ ions was extremely low (less than 0.1%), so, the right-hand polarized waves could also be excited locally. However, the exact mechanism for the polarization reversal remains unclear, and further efforts are necessary.

Resonance interaction is an effective energy conversion mechanism between particles and waves. But, this mechanism needs the energy of particles to be above the minimum resonant energy. For the EMIC waves, the minimum resonant energy of protons can be obtained by the resonance condition, $\frac{1}{2}m_p\left(\frac{\omega-\Omega_p}{k_\parallel}\right)^2$, where m_p is proton mass, Ω_p is proton gyrofrequency, ω is the frequency of EMIC waves, and $k_\parallel$ represents the parallel wavenumber of the EMIC waves, which can be got by the cold plasma dispersion relation (Baumjohann & Treumann, 1997). In our event, the minimum resonant energy of protons was estimated as 1.5 keV, which is much larger than the energy of cold protons studied in this paper, suggesting that the cold protons were not energized by the resonance interaction.

On the other hand, the non-resonance interaction has been proposed to describe the interaction between the cold ions and EMIC waves (Berchem & Gendrin, 1985; Q. M. Lu & Li, 2007; Mauk, 1982). When the velocity of ions, $\mathbf{V}_p$, is small, the electric force from the wave electric field, $q\mathbf{E}_{\text{wave}}$, will become comparable to the Lorentz force from the background magnetic field, $q\mathbf{B}_0\mathbf{V}_p$. Thus, the ions will be modulated by the wave electric field. The modulated ions will bunch into a small group and rotate together with the wave magnetic field, described as electric phase bunching. This process has also been used to describe the interaction between cold ions and low-frequency Alfven waves (Q. M. Lu & Li, 2007). The electric phase bunching can descript exactly our observation when the polarization of EMIC waves is left-hand (left column in Figure 3). The phase bunched cold protons followed the left-hand rotation of wave magnetic fields (Figure 3e), and the flux of bunched cold protons increased when the wave electric field was strong (Figure 3f), indicating that the bunched protons were modulated by the wave electric field, and the cold protons were energized by EMIC waves via non-resonance interaction.

However, when the EMIC waves were right-hand polarized, the bunched protons had a stable angle in the gyrophase (Figure 3k), which was different from the prediction from non-resonance interaction. Nevertheless, the bunched protons were still modulated by the wave electric field (Figure 3l), and the relative phase angles

between wave magnetic fields and bunched cold protons were similar to those in the left-hand polarized waves. It indicates that the cold ions may undergo a similar process to the non-resonance interaction when the EMIC waves were right-hand polarized.

The energy conversion rate ($\mathbf{J}_i \cdot \mathbf{E}_{wave}$) from EMIC waves to cold protons was calculated in this work (Figures 2d, 3c, and 3i), and the positive values indicate that the energy was transferred from EMIC waves to cold protons. It should be noted that the wave electric fields and the wave magnetic fields are not perfectly orthogonal (Figures 3f and 3l) in this event, and the relative angles between them were slightly less than 90°, which may be caused by the specific plasma condition (the related discussion can be found in Supporting Information S1). Thus, the energy conversion rates calculated in our work should be overestimated, and have a large uncertainty. However, as shown in Figures 3f and 3l, the most bunched protons were observed at the wave-phase angle between 0° and 90°. Therefore, even if the relative phase angles between $\mathbf{E}_{wave}$ and $\mathbf{B}_{wave}$ strictly equal to 90°, the relative angles between $\mathbf{E}_{wave}$ and the velocities of the most bunched cold protons were still less than 90°. Namely, the energy was indeed transferred from the EMIC waves to cold protons. Moreover, because the bunched protons were not uniform distribution during one wave period (Figures 3e and 3k), the current density (Figures 3d and 3j) and energy conversion rate (Figures 2d, 3c, 3i) showed some fluctuations, sometimes with two peaks in one wave period.

The EMIC waves could be observed in the magnetosphere over a large range of latitudes (Allen et al., 2015; Usanova et al., 2012). However, a statistical study showed that the cold ions energization events associated with EMIC waves were mainly observed at low/middle magnetic latitudes (Lee et al., 2021; J. C. Zhang et al., 2011). The reason for the contradiction may be that the intensity of EMIC waves at high latitudes is too weak to interact with the cold ions via the non-resonant interaction. In addition, the non-resonant interaction may also be affected by the magnetic mirror force at the high latitudes. The exact latitudinal range where the non-resonant interaction can occur and the effect of the mirror force on the interaction still need further statistical work.

In conclusion, we study the wave-particle interaction between the cold protons and EMIC waves with different polarizations. The cold protons were energized by the EMIC waves via the non-resonance interaction regardless of the wave polarization. The polarization of EMIC waves could change the gyrophase distribution of bunched cold protons, but the energy transfer process is not affected by the polarization of EMIC waves.

Data Availability Statement

All the MMS data used in this work are available at the MMS data center (https://lasp.colorado.edu/mms/sdc/public/about/browse-wrapper/). The data have been loaded, analyzed, and plotted using the SPEDAS software (Version 5.0) (Angelopoulos et al., 2019), which can be downloaded via the Downloads and Installation page (http://spedas.org/blog/).

Acknowledgments
This work is supported by the National Science Foundation of China (NSFC) grants (42174187), key research program of frontier sciences CAS (QYZDJ-SSW-DQC010), National Key Research and Development Program of China (2022YFA1604600), and the Fundamental Research Funds for the Central Universities. We thank Fuliang Xiao of Changsha University of Science and Technology and Zhigang Yuan of Wuhan University for the fruitful discussions. We thank the entire MMS team and instrument principal investigators for providing and calibrating data.

References

Allen, R., Zhang, J. C., Kistler, L., Spence, H., Lin, R. L., Klecker, B., et al. (2015). A statistical study of EMIC waves observed by Cluster: 1. Wave properties. *Journal of Geophysical Research: Space Physics*, *120*(7), 5574–5592. https://doi.org/10.1002/2015ja021333

An, X., Artemyev, A., Angelopoulos, V., Zhang, X. J., Mourenas, D., & Bortnik, J. (2022). Nonresonant scattering of relativistic electrons by electromagnetic ion cyclotron waves in Earth's radiation belts. *Physical Review Letters*, *129*(13), 135101. https://doi.org/10.1103/PhysRevLett.129.135101

Anderson, B. J., Erlandson, R. E., & Zanetti, L. J. (1992). A statistical study of Pc 1-2 magnetic pulsations in the equatorial magnetosphere. 1. Equatorial occurrence distributions. *Journal of Geophysical Research: Space*, *97*(A3), 3075–3088. https://doi.org/10.1029/91ja02706

Angelopoulos, V., Cruce, P., Drozdov, A., Grimes, E. W., Hatzigeorgiu, N., King, D. A., et al. (2019). The space physics environment data analysis system (SPEDAS) (Version 5.0) [Software]. Space Science Reviews, *215*(1), 9. https://doi.org/10.1007/s11214-018-0576-4

Baumjohann, W., & Treumann, R. A. (1997). *Advanced space plasma physics*. World Scientific.

Berchem, J., & Gendrin, R. (1985). Nonresonant interaction of heavy ions with electromagnetic ion cyclotron waves. *Journal of Geophysical Research*, *90*(A11), 10945–10960. https://doi.org/10.1029/ja090ia11p10945

Bortnik, J., Thorne, R., & Omidi, N. (2010). Nonlinear evolution of EMIC waves in a uniform magnetic field: 2. Test-particle scattering. *Journal of Geophysical Research*, *115*(A12), A12242. https://doi.org/10.1029/2010ja015603

Burch, J. L., Moore, T. E., Torbert, R. B., & Giles, B. L. (2016). Magnetospheric multiscale overview and science objectives. *Space Science Reviews*, *199*(1–4), 5–21. https://doi.org/10.1007/s11214-015-0164-9

Carson, B. R., Rodger, C. J., & Clilverd, M. A. (2013). POES satellite observations of EMIC-wave driven relativistic electron precipitation during 1998–2010. *Journal of Geophysical Research: Space Physics*, *118*(1), 232–243. https://doi.org/10.1029/2012ja017998

Chen, H., Gao, X., Lu, Q., Tsurutani, B. T., & Wang, S. (2020). Statistical evidence for EMIC wave excitation driven by substorm injection and enhanced solar wind pressure in the Earth's magnetosphere: Two different EMIC wave sources. *Geophysical Research Letters*, *47*(21), e2020GL090275. https://doi.org/10.1029/2020gl090275

Chen, H., Gao, X., Lu, Q., & Wang, S. (2019). Analyzing EMIC waves in the inner magnetosphere using long-term Van Allen Probes observations. *Journal of Geophysical Research: Space Physics*, *124*(9), 7402–7412. https://doi.org/10.1029/2019ja026965

Chen, L., Jordanova, V. K., Spasojević, M., Thorne, R. M., & Horne, R. B. (2014). Electromagnetic ion cyclotron wave modeling during the geospace environment modeling challenge event. *Journal of Geophysical Research: Space Physics*, *119*(4), 2963–2977. https://doi.org/10.1002/2013ja019595

Chen, L., Thorne, R. M., & Bortnik, J. (2011). The controlling effect of ion temperature on EMIC wave excitation and scattering. *Geophysical Research Letters*, *38*(16), L16109. https://doi.org/10.1029/2011gl048653

Chen, L. J., Thorne, R. M., Bortnik, J., & Zhang, X. J. (2016). Nonresonant interactions of electromagnetic ion cyclotron waves with relativistic electrons. *J Geophys ResSpace*, *121*(10), 9913–9925. https://doi.org/10.1002/2016ja022813

Cornwall, J. M. (1965). Cyclotron instabilities and electromagnetic emission in the ultra low frequency and very low frequency ranges. *Journal of Geophysical Research*, *70*(1), 61–69. https://doi.org/10.1029/jz070i001p00061

Denton, R. E., Hudson, M. K., & Roth, I. (1992). Loss-cone-driven ion cyclotron waves in the magnetosphere. *Journal of Geophysical Research*, *97*(A8), 12093–12103. https://doi.org/10.1029/92ja00954

Ergun, R. E., Tucker, S., Westfall, J., Goodrich, K. A., Malaspina, D. M., Summers, D., et al. (2016). The axial double probe and fields signal processing for the MMS mission. *Space Science Reviews*, *199*(1–4), 167–188. https://doi.org/10.1007/s11214-014-0115-x

Fukuhara, H., Kojima, H., Ueda, Y., Omura, Y., Katoh, Y., & Yamakawa, H. (2009). A new instrument for the study of wave-particle interactions in space: One-chip Wave-Particle Interaction Analyzer. *Earth Planets and Space*, *61*(6), 765–778. https://doi.org/10.1186/bf03353183

Gao, X., Li, W., Bortnik, J., Thorne, R. M., Lu, Q., Ma, Q., et al. (2015). The effect of different solar wind parameters upon significant relativistic electron flux dropouts in the magnetosphere. *Journal of Geophysical Research: Space Physics*, *120*(6), 4324–4337. https://doi.org/10.1002/2015ja021182

Gary, S. P., Liu, K., & Chen, L. (2012). Alfvén-cyclotron instability with singly ionized helium: Linear theory. *Journal of Geophysical Research*, *117*(A8), A08201. https://doi.org/10.1029/2012ja017740

Horne, R. B., & Thorne, R. M. (1997). Wave heating of He+ by electromagnetic ion cyclotron waves in the magnetosphere: Heating near the H+-He+ bi-ion resonance frequency. *Journal of Geophysical Research*, *102*(A6), 11457–11471. https://doi.org/10.1029/97ja00749

Hu, Y., & Denton, R. (2009). Two-dimensional hybrid code simulation of electromagnetic ion cyclotron waves in a dipole magnetic field. *Journal of Geophysical Research*, *114*(A12), A12217. https://doi.org/10.1029/2009ja014570

Hu, Y., Denton, R., & Johnson, J. (2010). Two-dimensional hybrid code simulation of electromagnetic ion cyclotron waves of multi-ion plasmas in a dipole magnetic field. *Journal of Geophysical Research*, *115*(A9), A09218. https://doi.org/10.1029/2009ja015158

Jordanova, V., Farrugia, C. J., Thorne, R., Khazanov, G., Reeves, G., & Thomsen, M. (2001). Modeling ring current proton precipitation by electromagnetic ion cyclotron waves during the May 14–16, 1997, storm. *Journal of Geophysical Research*, *106*(A1), 7–22. https://doi.org/10.1029/2000ja002008

Kang, N., Lu, Q., Gao, X., Wang, X., Chen, H., & Wang, S. (2021). Propagation of electromagnetic ion cyclotron waves in a dipole magnetic field: A 2-D hybrid simulation. *Journal of Geophysical Research: Space Physics*, *126*(12), e2021JA029720. https://doi.org/10.1029/2021ja029720

Kennel, C. F., & Petschek, H. (1966). Limit on stably trapped particle fluxes. *Journal of Geophysical Research*, *71*(1), 1–28. https://doi.org/10.1029/jz071i001p00001

Kim, E. H., & Johnson, J. R. (2016). Full-wave modeling of EMIC waves near the He+ gyrofrequency. *Geophysical Research Letters*, *43*(1), 13–21. https://doi.org/10.1002/2015gl066978

Kim, K. H., Kwon, H. J., Lee, J., Jin, H., & Seough, J. (2021). A case study of transversely heated low-energy helium ions by EMIC waves in the plasmasphere. *Journal of Geophysical Research: Space Physics*, *126*(2), e2020JA028560. https://doi.org/10.1029/2020ja028560

Kim, K. H., Takahashi, K., Lee, J., Jin, H., & Kwon, J. W. (2022). Mass density inferred from toroidal wave frequencies and energization of low-energy helium ions during H-band emic wave interval. *Journal of Geophysical Research: Space Physics*, *127*(8), e2022JA030523. https://doi.org/10.1029/2022ja030523

Kitamura, N., Kitahara, M., Shoji, M., Miyoshi, Y., Hasegawa, H., Nakamura, S., et al. (2018). Direct measurements of two-way wave-particle energy transfer in a collisionless space plasma. *Science*, *361*(6406), 1000–1003. https://doi.org/10.1126/science.aap8730

Kitamura, N., Shoji, M., Nakamura, S., Kitahara, M., Amano, T., Omura, Y., et al. (2021). Energy transfer between hot protons and electromagnetic ion cyclotron waves in compressional pc5 ultra-low frequency waves. *Journal of Geophysical Research: Space Physics*, *126*(5), e2020JA028912. https://doi.org/10.1029/2020ja028912

Lee, J., Kim, K. H., & Lee, E. (2021). A statistical study of low-energy ion flux enhancements by EMIC waves in the inner magnetosphere. *Journal of Geophysical Research: Space Physics*, *126*(8), e2021JA029793. https://doi.org/10.1029/2021ja029793

Li, J.-H., Liu, Z.-Y., Zhou, X.-Z., Li, L., Omura, Y., Yue, C., et al. (2022). Anomalous resonance between low-energy particles and electromagnetic plasma waves. *Communications Physics*, *5*(1), 300. https://doi.org/10.1038/s42005-022-01083-y

Li, W., Shprits, Y., & Thorne, R. (2007). Dynamic evolution of energetic outer zone electrons due to wave-particle interactions during storms. *Journal of Geophysical Research*, *112*(A10), A10220. https://doi.org/10.1029/2007ja012368

Lindqvist, P. A., Olsson, G., Torbert, R. B., King, B., Granoff, M., Rau, D., et al. (2016). The spin-plane double probe electric field instrument for MMS. *Space Science Reviews*, *199*(1–4), 137–165. https://doi.org/10.1007/s11214-014-0116-9

Liu, Z. Y., Zong, Q., Zhou, X., Hao, Y. X., Yau, A. W., Zhang, H., et al. (2019). ULF waves modulating and acting as mass spectrometer for dayside ionospheric outflow ions. *Geophysical Research Letters*, *46*(15), 8633–8642. https://doi.org/10.1029/2019gl083849

Liu, Z.-Y., Zong, Q.-G., Rankin, R., Zhang, H., Wang, Y., Zhou, X.-Z., et al. (2022). Simultaneous macroscale and microscale wave–ion interaction in near-earth space plasmas. *Nature Communications*, *13*(1), 5593. https://doi.org/10.1038/s41467-022-33298-6

Lu, Q., Guo, F., & Wang, S. (2006). Magnetic spectral signatures in the terrestrial plasma depletion layer: Hybrid simulations. *Journal of Geophysical Research*, *111*(A4), A04207. https://doi.org/10.1029/2005ja011405

Lu, Q. M., & Li, X. (2007). Heating of ions by low-frequency Alfven waves. *Physics of Plasmas*, *14*(4), 042303. https://doi.org/10.1063/1.2715569

Mauk, B. (1982). Electromagnetic wave energization of heavy ions by the electric "phase bunching" process. *Geophysical Research Letters*, *9*(10), 1163–1166. https://doi.org/10.1029/gl009i010p01163

McCollough, J., Elkington, S., & Baker, D. (2012). The role of Shabansky orbits in compression-related electromagnetic ion cyclotron wave growth. *Journal of Geophysical Research*, *117*(A1), A01208. https://doi.org/10.1029/2011ja016948

Meredith, N. P., Horne, R. B., Kersten, T., Fraser, B. J., & Grew, R. S. (2014). Global morphology and spectral properties of EMIC waves derived from CRRES observations. *Journal of Geophysical Research: Space Physics*, *119*(7), 5328–5342. https://doi.org/10.1002/2014ja020064

Ni, B., Cao, X., Zou, Z., Zhou, C., Gu, X., Bortnik, J., et al. (2015). Resonant scattering of outer zone relativistic electrons by multiband EMIC waves and resultant electron loss time scales. *Journal of Geophysical Research: Space Physics*, *120*(9), 7357–7373. https://doi.org/10.1002/2015ja021466

Omidi, N., Thorne, R., & Bortnik, J. (2010). Nonlinear evolution of EMIC waves in a uniform magnetic field: 1. Hybrid simulations. *Journal of Geophysical Research*, *115*(A12), A12241. https://doi.org/10.1029/2010ja015607

Omura, Y., Ashour-Abdalla, M., Gendrin, R., & Quest, K. (1985). Heating of thermal helium in the equatorial magnetosphere: A simulation study. *Journal of Geophysical Research*, *90*(A9), 8281–8292. https://doi.org/10.1029/ja090ia09p08281

Pollock, C., Moore, T., Jacques, A., Burch, J., Gliese, U., Saito, Y., et al. (2016). Fast plasma investigation for magnetospheric multiscale. *Space Science Reviews*, *199*(1–4), 331–406. https://doi.org/10.1007/s11214-016-0245-4

Rauch, J., & Roux, A. (1982). Ray tracing of ULF waves in a multicomponent magnetospheric plasma: Consequences for the generation mechanism of ion cyclotron waves. *Journal of Geophysical Research*, *87*(A10), 8191–8198. https://doi.org/10.1029/ja087ia10p08191

Russell, C. T., Anderson, B. J., Baumjohann, W., Bromund, K. R., Dearborn, D., Fischer, D., et al. (2016). The magnetospheric multiscale magnetometers. *Space Science Reviews*, *199*(1–4), 189–256. https://doi.org/10.1007/s11214-014-0057-3

Shi, C., Zhao, J., Huang, C., Wang, T., & Dunlop, M. W. (2020). Modulation of ionospheric outflow ions by EMIC waves in the dayside outer magnetosphere. *Physics of Plasmas*, *27*(3), 032902. https://doi.org/10.1063/1.5142686

Teng, S., Li, W., Tao, X., Ma, Q., Wu, Y., Capannolo, L., et al. (2019). Generation and characteristics of unusual high frequency EMIC waves. *Geophysical Research Letters*, *46*(24), 14230–14238. https://doi.org/10.1029/2019gl085220

Thorne, R. M., & Kennel, C. (1971). Relativistic electron precipitation during magnetic storm main phase. *Journal of Geophysical Research*, *76*(19), 4446–4453. https://doi.org/10.1029/ja076i019p04446

Usanova, M., Mann, I., Bortnik, J., Shao, L., & Angelopoulos, V. (2012). THEMIS observations of electromagnetic ion cyclotron wave occurrence: Dependence on AE, SYMH, and solar wind dynamic pressure. *Journal of Geophysical Research*, *117*(A10), A10218. https://doi.org/10.1029/2012ja018049

Xiao, F., Chen, L., He, Y., Su, Z., & Zheng, H. (2011). Modeling for precipitation loss of ring current protons by electromagnetic ion cyclotron waves. *Journal of Atmospheric and Solar-Terrestrial Physics*, *73*(1), 106–111. https://doi.org/10.1016/j.jastp.2010.01.007

Xiao, F., Zhou, Q., He, H., Zheng, H., & Wang, S. (2007). Electromagnetic ion cyclotron waves instability threshold condition of suprathermal protons by kappa distribution. *Journal of Geophysical Research*, *112*(A7), A07219. https://doi.org/10.1029/2006ja012050

Young, D., Perraut, S., Roux, A., De Villedary, C., Gendrin, R., Korth, A., et al. (1981). Wave-particle interactions near ΩHe+ observed on GEOS 1 and 2 1. Propagation of ion cyclotron waves in He+-rich plasma. *Journal of Geophysical Research*, *86*(A8), 6755–6772. https://doi.org/10.1029/ja086ia08p06755

Young, D. T., Burch, J. L., Gomez, R. G., De Los Santos, A., Miller, G. P., Wilson, P., et al. (2016). Hot plasma composition analyzer for the magnetospheric multiscale mission. *Space Science Reviews*, *199*(1–4), 407–470. https://doi.org/10.1007/s11214-014-0119-6

Yuan, Z., Xiong, Y., Wang, D., Li, M., Deng, X., Yahnin, A., et al. (2012). Characteristics of precipitating energetic ions/electrons associated with the wave-particle interaction in the plasmaspheric plume. *Journal of Geophysical Research*, *117*(A8), A08324. https://doi.org/10.1029/2012ja017783

Yuan, Z., Yu, X., Wang, D., Huang, S., Li, H., Yu, T., et al. (2016). In situ evidence of the modification of the parallel propagation of EMIC waves by heated He+ ions. *Journal of Geophysical Research: Space Physics*, *121*(7), 6711–6717. https://doi.org/10.1002/2016ja022573

Yue, C., Jun, C. W., Bortnik, J., An, X., Ma, Q., Reeves, G. D., et al. (2019). The relationship between EMIC wave properties and proton distributions based on Van Allen probes observations. *Geophysical Research Letters*, *46*(8), 4070–4078. https://doi.org/10.1029/2019gl082633

Zhang, J. C., Kistler, L., Mouikis, C., Klecker, B., Sauvaud, J. A., & Dunlop, M. (2011). A statistical study of EMIC wave-associated He+ energization in the outer magnetosphere: Cluster/CODIF observations. *Journal of Geophysical Research*, *116*(A11), A11201. https://doi.org/10.1029/2011ja016690

Zhang, X. J., Li, W., Ma, Q., Thorne, R., Angelopoulos, V., Bortnik, J., et al. (2016). Direct evidence for EMIC wave scattering of relativistic electrons in space. *Journal of Geophysical Research: Space Physics*, *121*(7), 6620–6631. https://doi.org/10.1002/2016ja022521

References From the Supporting Information

Zenitani, S., Hesse, M., Klimas, A., & Kuznetsova, M. (2011). New measure of the dissipation region in collisionless magnetic reconnection. *Physical Review Letters*, *106*(19), 195003. https://doi.org/10.1103/PhysRevLett.106.195003